EUROPEAN ORGANIZATION FOR NUCLEAR RESEARCH
European Laboratory for Particle Physics

Large Hadron Collider Project

LHC Project Report 914

Dynamic Stresses in the LHC TCDS Diluter from 7 TeV Beam Loading

B. Goddard, L. Massidda[1)], A. Presland, W. Weterings
CERN, Geneva, Switzerland

Abstract

In the event of an unsynchronised beam abort, the MSD extraction septum of the LHC beam dumping system is protected from damage by the TCDS diluter. The simultaneous constraints of obtaining sufficient beam dilution while ensuring the survival of the TCDS make the design difficult, with high thermally induced dynamic stresses occurring in the material needed to attenuate the particle showers induced by the primary beam impact. In this paper, full 3D simulations are described where the worst-case beam loading has been used to generate the local temperature rise and to follow the resulting time evolution of the mechanical stresses. The results and the accompanying design changes for the TCDS, to provide an adequate performance margin, are detailed.

1) CRS4, Sardina, Italy.

Presented at
EPAC'06, Edinburgh, UK,
June 26-30, 2006

CERN,
CH-1211 Geneva 23,
Switzerland
Geneva, June 2006

DYNAMIC STRESSES IN THE LHC TCDS DILUTER FROM 7 TEV BEAM LOADING

B.Goddard, A.Presland, W.Weterings, CERN, Geneva, Switzerland.
L.Massidda, CRS4, Sardina, Italy.

Abstract

In the event of an unsynchronised beam abort, the MSD extraction septum of the LHC beam dumping system is protected from damage by the TCDS diluter. The simultaneous constraints of obtaining sufficient beam dilution while ensuring the survival of the TCDS make the design difficult, with high thermally induced dynamic stresses occurring in the material needed to attenuate the particle showers induced by the primary beam impact. In this paper, full 3D simulations are described where the worst-case beam loading has been used to generate the local temperature rise and to follow the resulting time evolution of the mechanical stresses. The results and the accompanying design changes for the TCDS, to provide an adequate performance margin, are detailed.

BEAM DUMP DILUTER TCDS

To protect the beam dump extraction elements against particles in the abort gap and unsynchronised beam aborts, a fixed diluter TCDS [1] will be installed in front of the MSD extraction septum in the IR6 dump insertion. The TCDS is comprised of two 3.0 m long diluter blocks, with a graded composition to obtain the optimum compromise between absorbing power and robustness.

The ~24 mm diluter thickness has been chosen to protect the downstream septum elements and vacuum chambers from badly extracted beams. The TCDS must protect the MSD septum when the worst-case beam load occurs following a pre-trigger of one extraction kicker and the subsequent asynchronous triggering of the remaining 14 kickers. The TCDS must also survive the worst-case thermal load. The conceptual and mechanical designs have been based on FLUKA [2] energy deposition simulations, together with numerical and stress calculations made using a specially developed Finite Element (FE) code ELSE [3]. In particular, numerical analyses of dynamic effects were made on different TCDS configurations, and have resulted in an updated design with improved robustness.

The 6.0 m long unit is modelled as 24 separate 72×24×250 cm blocks, neglecting the slight differences in block widths and machining the entrance and exit blocks for beam impedance reasons.

ENERGY DEPOSITION SIMULATIONS

The energy deposition in TCDS element was calculated with FLUKA as input for the ELSE code. In the first case a single 7 TeV LHC ultimate proton bunch (1.7×10^{11} p+), with a beam size (1 σ) of 0.28mm and 0.34mm in the H and V planes was used, impacting at the axis of the TCDS. The total energy deposition was then calculated by superimposing this pattern 50 times on the TCDS mesh, using calculated bunch positions, with the 25 ns time structure. This approach does not take into account the fact that the real energy deposition profile will be different, as bunches impacting near the edges of the diluter will deposit less energy. In a second case the full sweep was modelled directly in FLUKA. The temperature profiles are slightly different, Fig. 1.

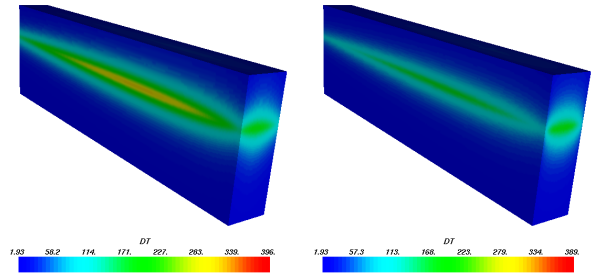

Figure 1. ΔT (K) in Ti block 23 for swept bunches at 25 ns intervals (left) and for instantaneous profile (right). The maxima are 401 and 389 K, respectively.

THERMO-ELASTIC SIMULATIONS

A detailed dynamic thermo-elastic analysis of the response of these types of structures is complex. The composite materials are anisotropic with significant differences in mechanical properties between the different directions; the beam size is small and produces a very local heating; finally, the beam passage is very rapid, producing a quasi-step increase in temperature and hence shock waves in the structure. To analyse this correctly requires details of the structural properties of the composite that must be determined with extensive testing, together with a large, multi-step, FE model.

The dynamic stresses depend on the material properties, the maximum value of the temperature and its distribution, and the rate of the temperature increase. In the case of the TCDS, the short 1 μs time scale of energy deposition means that dynamic effects are important.

Model

A linear elastic material model is assumed, with temperature-dependant material properties and no plastic deformation. For these short time scales, heat conduction inside the material can be neglected, as can heat conduction through the external surfaces. No material damping is considered, such that all approximations are conservative regarding the calculated stresses. The 3D mesh of the blocks consists of 51200 spectral elements with a spectral degree of 3, and an inter-nodal distance of between 0.2 and 2.0 mm, Fig. 2. The total number of degrees of freedom for the whole model was about 10^6.

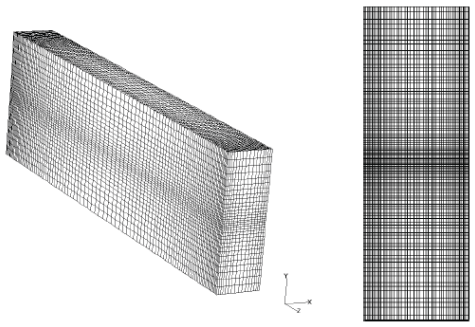

Figure 2. Simulation mesh (51200 nodes per block).

Individual analyses were run for each block, since in the TCDS device they are mechanically decoupled. All block surfaces were considered free, with the elastic energy confined within the block. Radiation and conduction were neglected. The time step of the simulation was 25 ns, equal to the inter-bunch interval.

The severity of the loading conditions of an individual block was estimated by comparing point-wise the computed stress at any given time to the material failure limit at the local temperature, expressed as a stress ratio. Isotropic materials were evaluated with the Stassi stress criterion, with the stress ratio defined as the computed Stassi tensile stress with the tensile strength of the material. For anisotropic materials the maximum stress criterion was used, where the stress ratio is the maximum of the ratio between each component of the stress tensor and the corresponding material strength, either compressive or tensile, at the temperature of the point.

The main simulations were performed for 11 of the 24 blocks (2, 4, 6, 8, 10, 13, 15, 17, 19, 22 and 24), because of their position in the diluter structure relative to the temperature profile and where the material changes.

SIMULATION RESULTS

Temperature increase

The temperature increase for the selected blocks is shown in Fig. 3, for the single bunch swept load. The temperature variation with position and material density is apparent, with the maximum at about z = 2.5 m. Of note are the big jump to the first Ti block (22) and the low temperature in the last steel block (24).

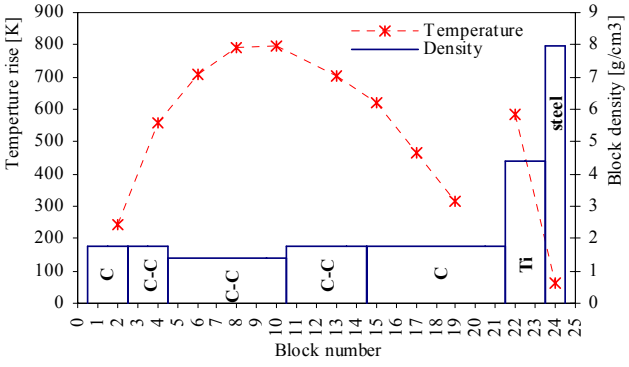

Figure 3. Temperature rise in selected blocks, for ultimate beam sweep. The material density variation is also shown.

The transverse evolution of the temperature profile along the diluter is as expected, becoming larger for downstream blocks as the shower develops. The temperature rise is not constant through the block in the sweeping direction (X), due to the varying sweep speed.

Propagation of stress waves

The compressive and tensile stresses form a complicated tensor stress wave, which can be resolved in X, Y and Z directions into σ_{yy}, σ_{xx} and σ_{zz} components. The beam heating causes a sudden temperature increase in the sweep plane, giving rise to two compressive stress waves for the σ_{yy} component, Fig. 4 centre, which travel outwards to the top and bottom free surfaces and are reflected back. The σ_{xx} component is directed along the sweep, and a compressive stress is caused by the thermal expansion in the sweep plane, with tensile stresses which develop from the lateral surfaces and travel towards the centre of the block. σ_{zz} behaves similarly, with tensile stress waves developing from the front and rear surfaces.

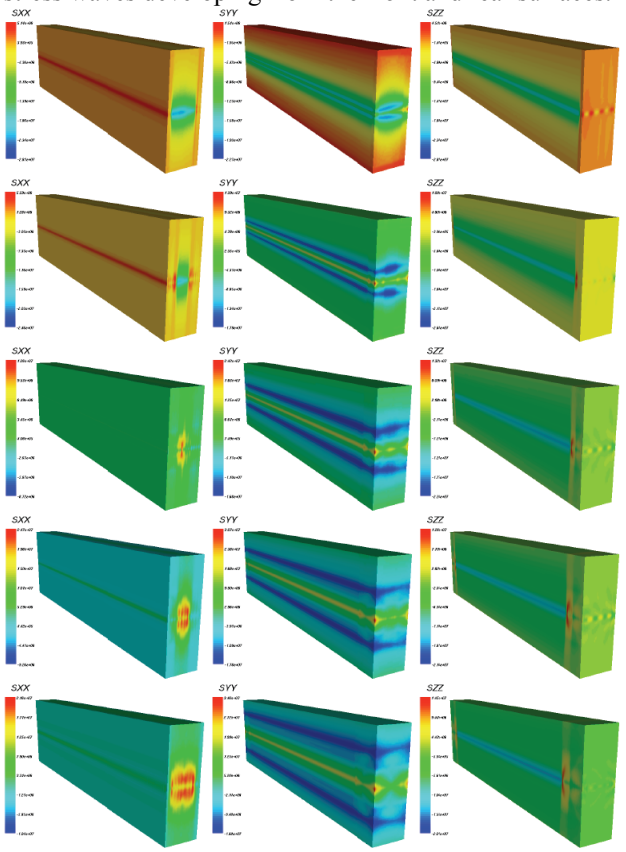

Figure 4. Evolution of σ_{yy}, σ_{xx} and σ_{zz} (left to right in block 15, for 2 - 10 μs (top to bottom) after beam impact.

Maximum stress ratios

The maximum value of the stress ratio for each point of the blocks was determined. Fig. 5 shows the results for blocks 15 (graphite) and 22 (Ti), and the maximum for any point on each block is shown along the diluter length in Fig. 8. The maxima are above the design limit of 1.0 for several blocks, including the final steel block where

the temperature rise is only 62 K. For the graphite blocks the σ_{yy} component is critical, Fig. 5 (left) with a localised stress peak at the intersection of the two vertical faces, where the two separate surface effects at the vertex are reinforced. Chamfering the edge would reduce this effect.

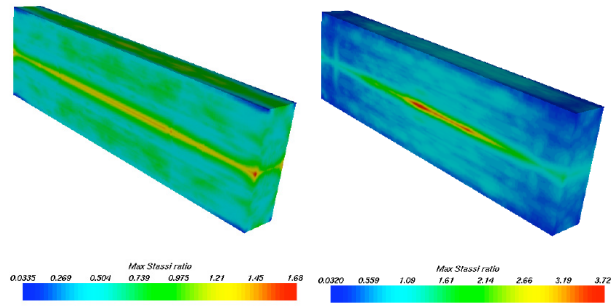

Figure 5. Maximum stress ratio over the 200 µs simulation for blocks 15 and 22.

The stress ratio was also evaluated as a function of time during the 200 µs of the simulation, Fig. 6. The initial stress ratio of about 0.6 can be seen to change dramatically as time evolves and the various waves reflect and interfere in different regions of the block. The peak value of 1.4 is over a factor of 2 above the value which one would estimate from a naive static approach.

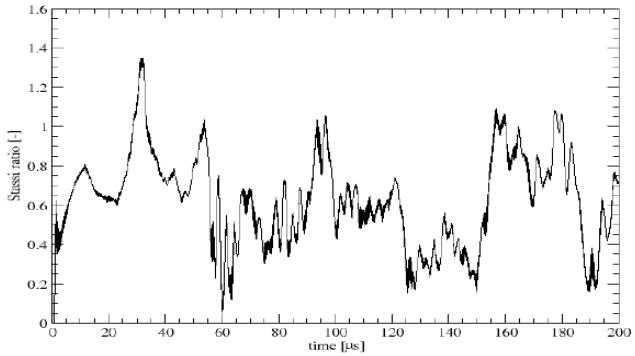

Figure 6. 200 µs evolution of stress ratio for block 15.

ADDITIONAL RESULTS

The effect of offsetting the beam impact vertically from the centre of the block was investigated. The centred and offset cases are shown in Fig. 7 for Ti block number 23, with a reduction of about 20% in the peak stress ratio.

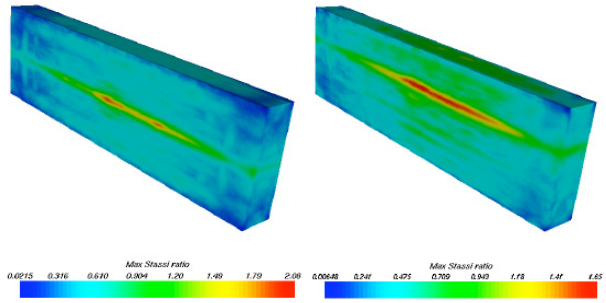

Figure 7. Stress ratio in block 23 (Ti) for centred and +1mm offset beam impact.

The effect of the real swept beam energy deposition profile was investigated, with a simultaneous deposition of all the beam energy at the start of the simulation. The resulting temperature profile was slightly different, as noted above, but the stress ratios derived from the analysis were comparable.

DILUTER OPTIMISATION

The results and method were used to optimise the TCDS design. All the highly stressed graphite blocks were replaced with high density C-C, which has much better mechanical properties. An additional C-C block was placed in front of the two Ti blocks, and the final steel block was dropped altogether. The performance of the new configuration was calculated using the same method, and also checked concerning the protection of the MSD septum. The comparison in the maximum stress ratios for the old and new configurations is shown in Fig. 8. All the graphite and C-C blocks are now below the design limit of 1.0 – however, the first Ti block (23) still has a stress ratio of about 1.5. This means that the material may exhibit plastic deformation for the impact of beam intensities above LHC nominal (1.15×10^{11} p+ per bunch); however, the resulting mechanical deformation will remain below the ±0.05 mm level, and can be tolerated for a few such failures.

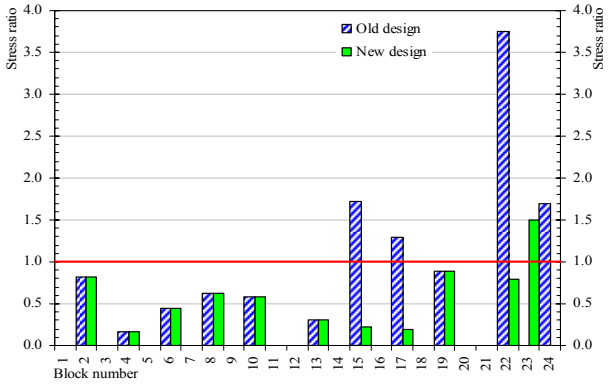

Figure 8. Comparison of maximum stress ratios between old and new designs.

CONCLUSION

The dynamic thermo-mechanical stress analyses have been analysed in detail and were essential in understanding the behaviour and optimising the design of the TCDS diluter. The studies show that this element is highly stressed under the assumed load conditions. A new design was developed which should now withstand nominal LHC beam; upgrade of the system for ultimate LHC intensity may still be required.

REFERENCES

[1] B.Goddard, M.Sans and W.Weterings, proceedings EPAC'04, Lucerne, 2004.

[2] A. Fassò et al., MonteCarlo 2000, Springer-Verlag Berlin, p. 955-960, 2001.

[3] F.Casadei et al., Comput. Methods Appl. Mech. Energ., 191, 5119-5148, 2002.